Research Article

Interfacial state induced ultrasensitive ultraviolet light photodetector with resolved flux down to 85 photons per second

Yong-Qiang Yu[1], Lin-Bao Luo[1] (✉), Ming-Zheng Wang[1], Bo Wang[1], Long-Hui Zeng[1], Chun-Yan Wu[1], Jian-Sheng Jie[2] (✉), Jian-Wei Liu[3], Li Wang[1], and Shu-Hong Yu[3] (✉)

[1] *School of Electronic Science and Applied Physics, Anhui Provincial Key Laboratory of Advanced Functional Materials and Devices, Hefei University of Technology, Hefei, Anhui 230009, China*

[2] *Institute of Functional Nano & Soft Materials (FUNSOM) and Jiangsu Key Laboratory for Carbon-Based Functional Materials & Devices, Soochow University, Suzhou, Jiangsu 215123, China*

[3] *Division of Nanomaterials & Chemistry, Hefei National Laboratory for Physical Sciences at Microscale, Department of Chemistry, University of Science and Technology of China, Hefei 230026, China*

ABSTRACT

We present an ultrasensitive ultraviolet (UV) detector based on a p-type ZnS nanoribbon (NR)/indium tin oxide (ITO) Schottky barrier diode (SBD). The device exhibits a pseudo-photovoltaic behavior which can allow the SBD to detect UV light irradiation with incident power of 6×10^{-17} W (~85 photons/s on the NR) at room temperature, with excellent reproducibility and stability. The corresponding detectivity and photoconductive gain are calculated to be 3.1×10^{20} cm·Hz$^{1/2}$·W^{-1} and 6.6×10^{5}, respectively. It is found that the presence of the trapping states at the p-ZnS NR/ITO interface plays a crucial role in determining the ultrahigh sensitivity of this nanoSBDs. Based on our theoretical calculation, even ultra-low photon fluxes on the order of several tens of photons could induce a significant change in interface potential and consequently cause a large photocurrent variation. The present study provides new opportunities for developing high-performance optoelectronic devices in the future.

1 Introduction

Ultraviolet (UV) detection has been receiving considerable attention lately for its wide applications including emitter calibration, flame sensors, spatial optical communications, and biological and chemical sensors [1]. Many important fields, such as quantum information and quantum optics [2], require highly sensitive detectors to distinguish UV signals with ultra-low photon fluxes on the order of single to hundreds of photons from the background. Currently, a variety of UV photodetectors including

---

Address correspondence to Linbao Luo, luolb@hfut.edu.cn; Jiansheng Jie, jsjie@suda.edu.cn; Shu-Hong Yu, shyu@ustc.edu.cn

photomultiplier tubes (PMT) [3], avalanche photodiodes (APDs) [4–6], and superconducting single-phonon detectors (SSPDs) [7, 8] are available for such purposes. PMTs have been often used because of their high responsivity, high speed, and low dark current. However, they are expensive and bulky, and require high operation voltage bias. On the other hand, semiconductor based APDs have been widely utilized due to their small footprint, ruggedness, excellent potential and inherently high gain and speed. Nevertheless, unfortunately, due to their limited stable gain, low quantum efficiency, high excess noise, and long dead time, APDs are quickly becoming the bottleneck in many applications. With regard to SSPDs, they need a critical operation temperature as low as 4 K, which makes them commercially unavailable at present.

In light of the apparent deficiencies mentioned above, attention has focused on new nanodevices based on semiconductor nanostructures, in an effort to achieve high-performance UV photodetectors with high quantum efficiency, low cost, and low-power consumption [9–14]. For instance, one-dimensional (1D) nanostructures have shown great potential in developing nano-photodetectors with high sensitivity for nanophotonic system applications [15–17]. By reducing the InP sensing volumes through a top-down etching technique, the rod-like photodiode can exhibit ultrasensitivity with very high gain at low bias. It was revealed that the entrapment of carriers in the nanorod structure can lead to a large potential change and thus produce an amplified electron injection [18, 19]. What is more, it has been found that 1D nanostructures fabricated by bottom-up growth usually possess high crystallinity as well as large surface-to-volume ratio. The surface energy band bending resulting from deep level surface traps can facilitate the separation of photo-generated carriers and, consequently, a longer photo-carrier lifetime is attained [20, 21]. By this token, a number of UV photoconductors constructed from wide band-gap semiconductor nanostructures such as ZnS nano-ribbons (NRs) [22, 23], ZnO nanowires (NWs) [20], and GaN NWs [21, 24, 25] with high internal photoconductive gain have been reported. In spite of these efforts, little work has been carried out with

respect to UV nano-photodetectors with resolution down to the level of tens of photons per second.

Herein, we present the fabrication of an ultrasensitive nano-photodetector for ultraviolet detection at room temperature. The device showed significant response to extremely weak UV light illumination (6×10^{-17} W, ~85 photons per second on the NR) at a bias voltage of 0.01 V, giving rise to detectivity and photoconductive gain as high as 3.1×10^{20} cm·Hz$^{1/2}$·W^{-1} and 6.6×10^{5}, respectively. The large potential variation caused by the photo-carrier trapping at the p-ZnS NR/indium tin oxide (ITO) interface was responsible for the extraordinary photo-sensitivity of the nano Schottky barrier diode (nanoSBD). The realization of p-ZnS NR/ITO SBD ultrasensitive photodetectors opens up huge opportunities for a host of important applications in nano-photonics and quantum information.

2 Experimental

2.1 Synthesis and characterization of the p-type ZnS:Ag NRs

The synthesis of the p-type ZnS NRs was carried out in a horizontal tube furnace using a thermal co-evaporation method. Briefly, 0.3 g of ZnS powder (99.99%, Aldrich) was loaded into an alumina boat and transferred to the center region of the furnace. Another boat loaded with Ag_2S powder (99.9%, Aldrich) was then placed in the upstream direction at a distance of 10 cm from the ZnS source. The molar ratio of Ag_2S:ZnS was 1:7. Several silicon substrates coated with 5 nm gold catalyst were located in the downstream direction 12 cm from the ZnS source. The evaporation system was evacuated to a base pressure of 4×10^{-5} Torr, and then backfilled with a constant H_2 (5% in Ar) gas flow of 40 sccm (standard-state cubic centimeters per minute) to 100 Torr. Afterwards, the ZnS source was heated to 1,060 °C in one hour and maintained at that temperature for 30 min. The temperatures of the Ag_2S source and Si substrates were ~950 °C and ~800 °C, respectively, during the growth. A layer of white wool-like product could be observed on the Si substrate surface after the reaction. Ag-doped ZnS NRs were characterized by scanning electron microscopy (SEM, Philips XL

30 FEG) equipped with an X-ray energy dispersive spectrometer (EDS) and cathodoluminescence (CL) system, high-resolution transmission electron microscopy (HRTEM, JEOL JEM-2010), and X-ray photoelectron spectroscopy (XPS, Thermo ESCALAB 250).

2.2 Device fabrication and characterization

In order to assess the electrical transport properties of the ZnS:Ag NRs, devices based on individual NRs were constructed. The NRs were first dispersed onto the SiO_2 (300 nm)/p^+-Si substrate, and then Cu (4 nm)/Au (60 nm) double-layer source and drain electrodes were fabricated by photolithography and subsequent lift-off process. As for the nanoSBDs, ITO electrodes (80 nm) served as the Schottky contacts and were defined by an additional photolithography process. A pulsed laser deposition (PLD) system with a KrF excimer laser (Lambda Physik COMPexPro 102,248 nm, 120 mJ, 5 Hz) was used to deposit the ITO film. The optimized deposition condition of ITO was found to be that the PLD deposition system kept a base pressure of 10 Pa without filled oxygen flow and the deposition rate was about 3 nm per min. Electrical characterization of the devices was performed using

a semiconductor characterization system (Keithley 4200-SCS) at room temperature. The capacitance versus voltage (C–V) and interface conductance versus frequency (G_{ss}–f) measurements were conducted by using a Keithley 4200-CVU system. The UV source was a commercially available UV light-emitting diode (LED) with a narrow band width of 275–285 nm peaking at 280 nm (SET. Inc., SET-N280). The power of the UV LED was ~100 µW under the test bias of 5.2 V. The light illumination intensity, i.e., the photon numbers that reached the NR could be tuned by adjusting the distance between the LED and the p-ZnS NR/ITO SBDs. The LED was turned ON/OFF manually to monitor the time response of the nanoSBDs.

3 Results and discussion

The ZnS:Ag NRs used in this study are of wurtzite structure, with width in the range of 100 nm–2 µm (Figs. 1(a) and 1(b)). According to the CL spectrum analysis, the NRs show a strong emission peaking at ~450 nm, which is seldom observed for intrinsic ZnS NRs [26]. Figure 1(d) shows a schematic illustration of the nano-device which consists of a long single-crystal
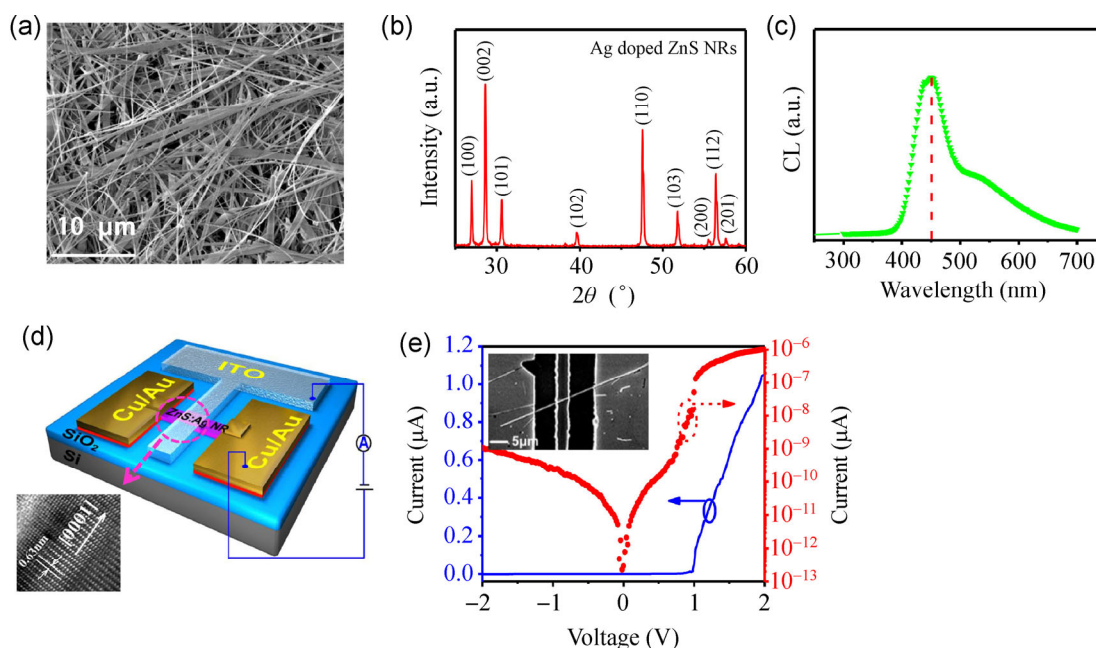

Figure 1 (a) A typical SEM image of the as-synthesized ZnS:Ag NRs. (b) XRD pattern of the ZnS:Ag NRs. (c) CL spectrum of the ZnS:Ag NRs. (d) Schematic illustration of the p-ZnS NR/ITO SBD; the inset shows a typical HRTEM image of the NR. (e) Typical rectifying curve of the nanoSBD in both semi-logarithmic and linear plots; the inset shows a typical SEM image of the nanoSBD.

[0001] oriented ZnS:Ag NR, two parallel Cu/Au electrodes at both ends, and one ITO electrode in the middle of the NR. The current–voltage curve of the Cu/Au/p-ZnS NR/ITO junction in the dark is plotted in Fig. 1(e), from which a pronounced rectification characteristic with a turn-on voltage of ~0.8 V and a rectification ratio of ~10^3 at ±3 V are observed. This behavior can be ascribed to the p-ZnS NR/ITO Schottky junction considering the formation of an Ohmic contact at Cu/Au/p-ZnS NR, which is attributed to the generation of a highly conductive Cu_2S interfacial layer at NR-Cu/Au [27]. Fitting the *I–V* characteristics leads to an ideality factor of 3.8, and a barrier height of 0.4 eV (see the Electronic Supplementary Material (ESM)). This relatively large ideality factor and the low barrier height are believed to be associated with the voltage drop at an interfacial layer which is formed between the p-ZnS:Ag NR and the ITO electrode during ITO deposition.

As established in a previous study, for such a metal–insulator–semiconductor (MIS) structure [28, 29],

the interfacial states may result in the band bending and behaving as recombination centers that support trap-assisted tunneling current, leading to the large ideality factor, high reverse current, and nonideal *I–V* characteristics [30]. In fact, the presence of the high density interfacial states is experimentally corroborated by the obvious hysteresis loop, when the device was subjected to a sequential voltage sweeping from –5 to +5 V, and then back to –5 V (Fig. 2(a) and Fig. S1 in the ESM).

Surface adsorption of gas molecules like water as well as the surface states originating from dangling bonds and defects normally account for the electrical hysteresis observed for semiconductor nanostructures [31]. In order to clarify the origin of the hysteresis in the p-ZnS NR/ITO SBDs, controlled experiments under various conditions were conducted (Fig. 2). It is found that reciprocating scans on a single ZnS:Ag NR with Ohmic contacts (Cu/Au electrodes) at two ends do not show any detectable hysteresis no matter what voltage sweeping speed is used (Figs. 2(b) and
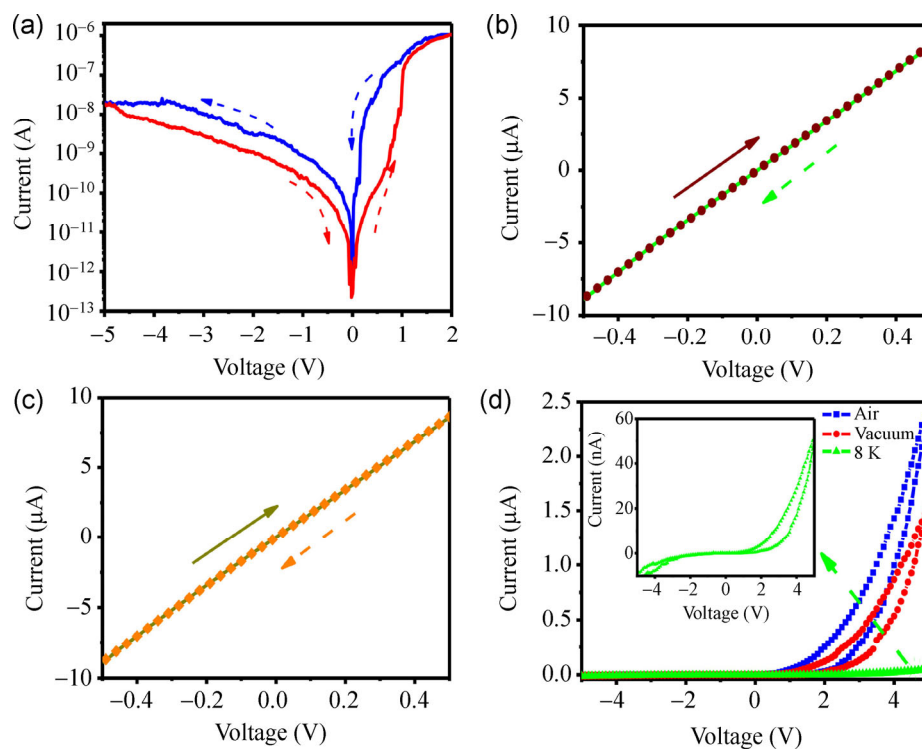

Figure 2　(a) Typical hysterisis loop of the nanoSBD in a semi-logarithmic plot. The arrows indicate the voltage sweeping direction. (b) *I–V* curves of ZnS:Ag NR/Cu/Au measured at voltage sweeping speed of 0.5 V·s^{-1}; the arrows indicate the voltage sweeping direction. (c) *I–V* curves of ZnS:Ag NR/Cu/Au measured at voltage sweeping speed of 0.05 V·s^{-1}; the arrows indicate the voltage sweeping direction. (d) Rectifying curves of the p-ZnS NR/ITO SBD measured in air, vacuum, and at low temperature (8 K) (Janis CCS-350). The inset shows the enlarged rectifying curve at 8 K. Large hysteresis is observed under all these conditions.

2(c)). This finding, combined with the well-retained hysteresis in vacuum or at low temperature, excludes the possibility that the observed hysteresis is due to surface adsorption (Fig. 2(d)). In the light of this, it is safe to conclude that the hysteresis stems from the interface states of the p-ZnS:Ag NR and ITO. Due to abundant interface states, electron trapping and detrapping at the interface will result in the large hysteresis of the device, which is similar to that observed for nonvolatile memory [32]. As a matter of fact, this assumption is also verified by examining metal–semiconductor-field-effect-transistors (MESFETs) based on the p-ZnS:Ag NR/ITO Schottky junction, in which a pronounced hysteresis loop was observed in the source–drain current (I_{ds}) versus V_g curve when applying the gate voltage (V_g) on the ITO electrode (see Fig. S1 in the ESM).

The photoresponse characteristics of the p-ZnS NR/ITO SBDs were evaluated by using a 280 nm UV LED, whose intensity can be readily adjusted by changing the distance between the light and nano-device (Fig. 3). As illustrated in Fig. 3, in this study, the UV LED source (280 nm, SET. Inc., SET-N280) with
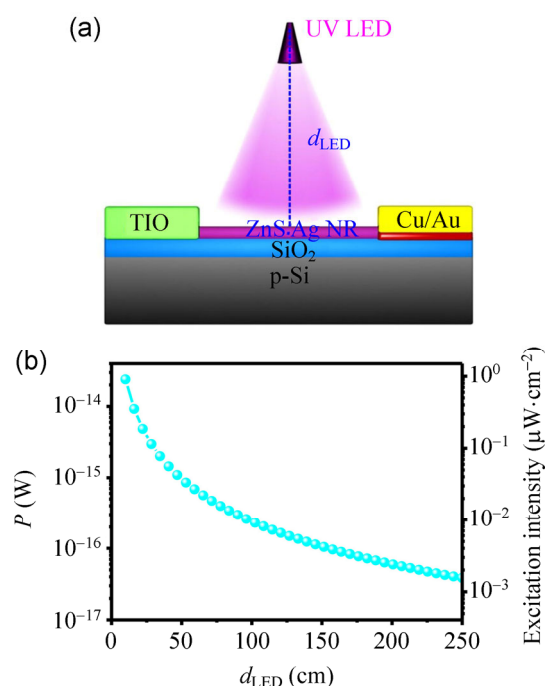

Figure 3 (a) Schematic illustration showing the experimental setup for measuring the photoconductive characteristics of the p-ZnS NR/ITO SBD. (b) Plot of the light power/intensity versus distance between the UV LED and the nanoSBD.

emission area ~1 mm² can be regarded as a point light source. The UV light power irradiated on the NR can be expressed as Eq. (1):

$$P = \frac{P_{light}}{d_{LED}^2} A_{NR} \tag{1}$$

where P_{light} is the UV LED power (100 μW), d_{LED} the distance between the UV LED and the nanoSBD, A_{NR} the area of the ZnS:Ag NR exposed to the UV light (~2.4 × 10⁻⁸ cm², according to the width of 400 nm and length of 6 μm for the NR). Therefore, the excitation power can be readily tuned by changing the d_{LED}.

Figure 4(a) plots the I–V curves of a typical nanoSBD measured in the dark and under UV illumination. Interestingly, when irradiated by a weak UV light with intensity of 1 μW·cm⁻², the nanoSBD device exhibits a pseudo-photovoltaic behavior with a positive short-circuit current (I_{sc}) of 2.0 nA and a negative open-circuit voltage (V_{oc}) of –1.0 V. This abnormal finding suggests that a different mechanism is involved during the separation and transfer of photo-generated carriers. Though the reason is unclear at this stage, this phenomenon can allow the detection of ultra- weak UV light illumination. The green curve in Fig. 4(b) plots the photoresponse of the nanoSBD measured at 0.01 V when the UV light was switched on and off. It can be seen that the nanoSBD photodetector can be reversibly switched between high and low conduction states, with excellent reproducibility. The I_{light}/I_{dark} ratio is determined to be ~10³, and the rise and fall time are both less than 1 s. Notably, even when the light intensity is reduced to 2.5 nW·cm⁻² (corresponding to 6 × 10⁻¹⁷ W, i.e., ~85 photons/s on the NR), the corresponding I_{light}/I_{dark} ratio is as high as 10, indicative of the ultrasensitivity of the nanoSBD device. We believe such a sensitivity can be further enhanced to tens of photons, or even to a single photon, if the device structures are appropriately optimized.

Both the gain (G) and the detectivity (D^*), two important metrics that are normally used to evaluate photodetector performance were estimated from the red curves shown in Fig. 4(c) (see also the ESM). The gain is calculated to be 6.6 × 10⁵, much higher than that of ZnS bulk and film photodetectors (~0.3) [1]. In contrast, conventional photovoltaic type photodetectors

have a photoconductive gain that is usually less than 1. As we will discuss later, this ultrahigh gain is probably due to the different operation mechanism involved during the photon detection process. In addition, the detectivity at 0.01 V is estimated to be 3.1×10^{20} cm·Hz$^{1/2}$·W^{-1} under light intensity of 2.5 nW·cm^{-2}. The D^* value in this work is significantly higher than that of PMTs, SiC APDs, and SSPD. Table 1 summarizes the key parameters of the p-ZnS NR/ITO based UV detector and other conventional detectors. Clearly, one can see that although the number of resolved photons of the present nanoSBD detector without

any optimization is inferior to other single-photon detectors, it is undeniable that our nanoSBD device offers two advantages: (1) Low operation voltage. Thanks to the pseudo-photovoltaic effect mentioned above, our device can work as an efficient photo-detector at a low bias voltage of 0.01 V. This is completely different from traditional commercial devices such as PMT or SiC APD, which normally require a bias voltage as high as 100 V. (2) Small device size. The device is mainly made of small-sized nanoribbons, rather than bulk or thin film as building blocks. As a result, the size of our device is only ~2.4 μm^2, much
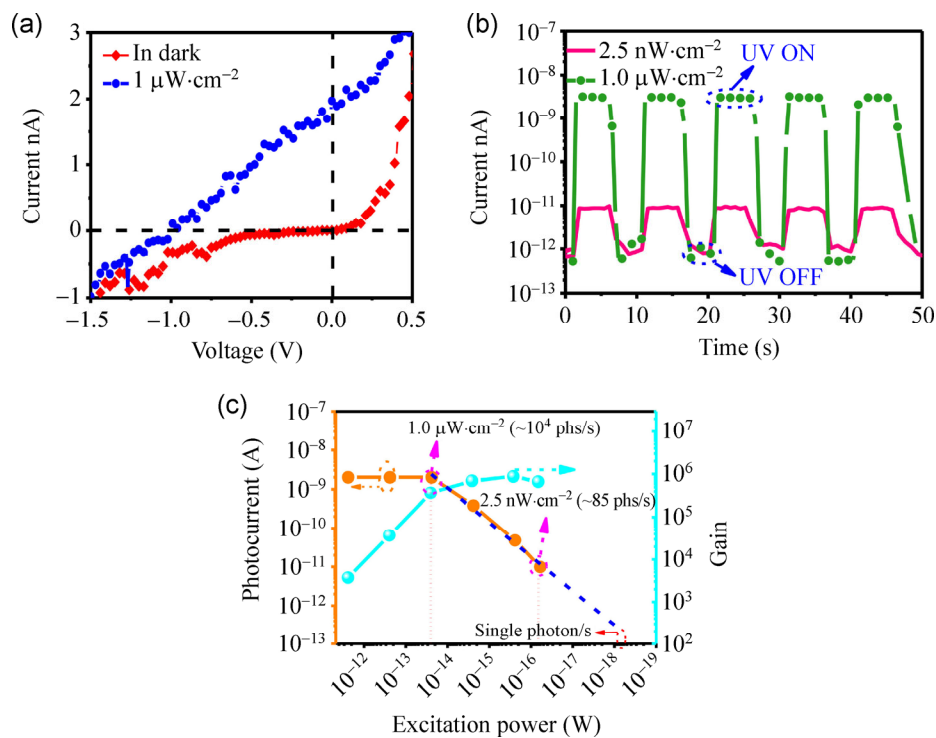

Figure 4 (a) *I–V* curves of the nanoSBD measured in dark and under UV light intensity of ~1 μW·cm^{-2}. (b) Time response of the nanoSBD measured under UV light intensities of 1 μW·cm^{-2} and 2.5 nW·cm^{-2}. The external bias voltage is fixed at 0.01 V. (c) The photocurrent and the photoconductive gain of the p-ZnS NR/ITO SBD as a function of excitation UV light intensity at an external bias voltage of 0.01 V; phs/s denotes photons/s.

Table 1 Comparison of the p-ZnS NR/ITO SBD based UV detector with other conmercial devices

Detector type	Operation voltage (V)	Operation temperature (K)	Size	Gain	Number of photons resolved	Detectivity (cm·Hz$^{1/2}$·W^{-1})
p-ZnS NR/ITO nanoSBDs	~0.01	300	2.4 μm^2	6.6×10^5	<85	3.1×10^{20}
PMTs [2, 3, 5]	~1,000	300	>1 cm^2	10^6–10^7	1	~10^{17}
SiC APDs [4, 5]	40–100	300	~100 μm^2	<10^6	>10^3	<10^{16}
SSPD [7, 8]	~0.01	<4	~10–100 μm^2	~10^7	1	<10^{17}

smaller than those of the three commercial devices listed in Table 1. These obvious merits, along with the ambient working temperature (300 K) render the present nanoSBD a promising candidate for application in future optoelectronic devices.

To unveil the physical origin of the ultrasensitivity, cyclic voltammetry (CV) analysis of the p-ZnS NR/ITO SBDs was carried out. As shown in Fig. 5(a), the heterojunction exhibits typical characteristics of a p-type semiconductor with a typical MIS structure [33]: The capacitance remains nearly constant at low voltage because of the presence of the insulating layer (interface layer), but decreases steeply when the depletion region in the p-ZnS NR expands. As the voltage further increases, an inversion layer will be formed on the ZnS NR surface and thus an enhanced capacitance is observed. Figure 5(b) shows the G_{ss}/ω versus ω ($\omega = 2\pi f$) curve on a semi-logarithmic scale at a forward bias voltage of +0.5 V. The interface state density can be deduced from the G_{ss}/ω versus ω curve by using the following expression [29, 34]

$$\frac{G_{ss}}{\omega} = \frac{SqD_{it}}{2\omega\tau}\ln(1+\omega^2\tau_{it}^2) \qquad (2)$$

where S is the diode contact area, and τ_{it} the time constant of the interface states. At the peak position $\omega = 2.5 \times 10^7\,\mathrm{S}^{-1}$, $\dfrac{\mathrm{d}(G_{ss}/\omega)}{\mathrm{d}(\omega)} = 0$, therefore D_{it} is calculated to be $1.77 \times 10^7\,\mathrm{cm}^{-2}\cdot\mathrm{eV}^{-1}$. These trapping states may originate from the surface defects on the ZnS NR or the oxide vacancies formed during ITO deposition process. They normally have a donor-like nature and play an important role in determining the ultrasensitivity of the nanoSBDs (Fig. 4(c)).

Upon UV light illumination, electron–hole pairs are generated within the p-ZnS NR, as a consequence of bandgap excitation. The electrons drift towards the interface due to the presence of the built-in and external electric fields and will then be captured by the trapping states.

Figure 5(c) schematically illustrates this trapping process for the photo-generated electrons at the p-ZnS NR/ITO interfacial layer. Due to the negative potential caused by the trapped electron(s) (Fig. 5(d)), the energy band at the p-ZnS NR side tends to bend downwards. Consequently, the Schottky barrier for the hole transport is reduced, leading to a positive conduction current from p-ZnS NR to ITO under UV light
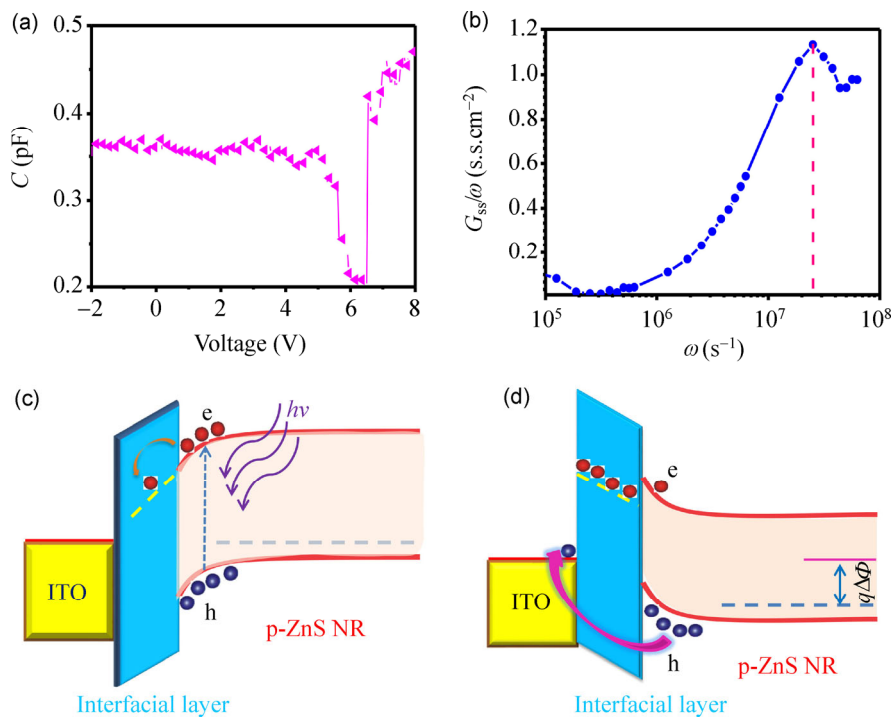

Figure 5 (a) C–V curve of the nanoSBD measured at a frequency of 1 MHz. (b) G_{ss}/ω vs. ω curve at bias voltage of +0.5 V. (c) Energy band diagram of the device before electron trapping. (d) Energy band diagram of the device after electron trapping.

illumination at 0.01 V. In this case, the carrier lifetime in high-crystal p-ZnS NR was considerably prolonged, which allows more holes to pass through the junction in a certain time. Although this model is quite different from conventional photovoltaic type photodetectors, in which a negative photocurrent in the circuit is formed as electrons drift to the n-type semiconductor side and holes drift into the p-type semiconductor, it explains well the abnormal positive photocurrent and the large photoconductive gain observed on the p-ZnS NR/ITO SBDs.

By using an abrupt approximation [33], the width of the band-bending induced depletion layer can be estimated to be 140 nm (see the ESM). For convenience, the depletion region was divided into two areas (Fig. 6(a)), i.e., Area 1 and Area 2, corresponding to the area beneath the ITO electrode and the area exposed to ambient, respectively. The properties of Area 1 can be expressed by the two-dimensional (2D) Poisson equation (Eq. (3))

$$\frac{\partial^2 \psi_1(x,y)}{\partial^2 x^2} + \frac{\partial^2 \psi_1(x,y)}{\partial^2 y^2} = -\frac{qN_{ZnS}}{\varepsilon_{ZnS}} \quad \text{for} \quad \begin{array}{l} 0 \leqslant x \leqslant L_g, \\ 0 \leqslant y \leqslant T_{ZnS} \end{array} \tag{3}$$

where ε_{ZnS} is the permittivity of Z_{nS}, N_{ZnS} the doping level, T_{ZnS} the thickness of the ZnS NR. The potential distribution can be obtained by solving the 2D and

1D Poisson equations for Area 1 and Area 2 with boundary conditions, respectively (See the ESM for the detailed solution of the Poisson equations). Figure 6(b) shows the potential and electric field distribution of the junction. It can be clearly seen that the depletion region exhibited an extended scope, not limited to the region under the ITO electrode, which is different from a traditional Schottky junction. The extended depletion region on NR was attributed to the thickness of the NR, which is less than the depletion layer width (d). Therefore, it is reasonable to assume that A_{eff} is close to the cross section area of the NR (~400 nm × 80 nm), as opposed to the full contact area of ITO with the NR. For such an interfacial state induced ultrasensitive nanoUVPD, UV light irradiation can induce a potential ($\Delta\phi$) at the interface which can be described as [35, 36]:

$$\Delta\phi = \frac{Q_{ss}d}{2A_{eff}\varepsilon_{ZnS}} \tag{4}$$

where Q_{ss} is the trapped charge. According to Eq. (4), a light intensity of 2.5 nW·cm⁻² can generate a potential variation of ~0.3 V, about ten times that of thermal fluctuation energy of carriers at room temperature (~26 meV). This means that even several tens of electrons could cause amplified hole injection from the p-ZnS NR to the ITO electrode [18, 19]. Due to limited interface states, the trapping states are completely occupied at light intensities higher than a certain saturation value (W_{sat}, ~1 μW·cm⁻²). In this state, the photocurrent tends to saturate, irrespective of any further increase of light intensity. In contrast, at lower light intensity, photocurrent will decrease with decreasing light intensity (Fig. 4(c)). This observation is consistent with the partial occupation of trapping states and the resulting decrease in interface potential.

4   Conclusions

We have demonstrated an ultrasensitive UV detector based on Ag-doped p-type ZnS NR/ITO SBD at 0.01 V. The detectivity and photoconductive gain for the device are as high as 3.1×10^{20} cm·Hz$^{1/2}$·W⁻¹ and 6.6×10^5, respectively, thus offering the capability to detect ultra-weak UV light (6×10^{-17} W, ~85 photons/s
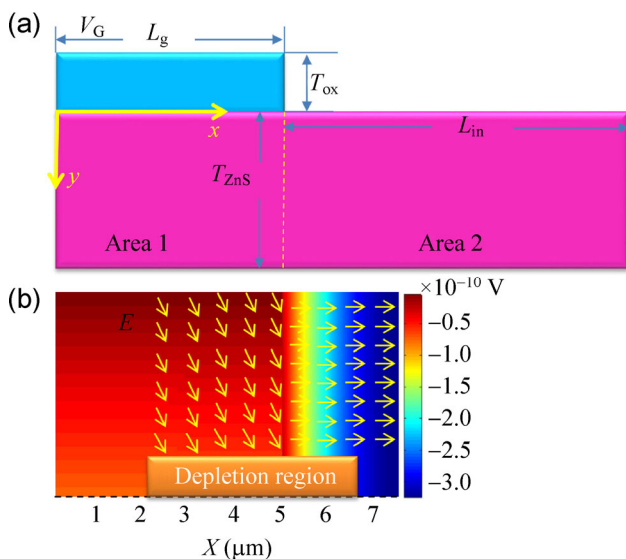

Figure 6 (a) Schematic demonstration of the p-type ZnS NR/ITO SBD. (b) The corresponding potential and electric field distribution in the depletion region.

on the NR) at room temperature. It has been shown that the trapping of photo-generated carriers at the p-ZnS NR/ITO interface can induce a large potential variation, which accounts for the extraordinary photo-sensitivity of the device. Our work demonstrates that the 1D semiconductor nanostructures are promising building blocks for construction of highly sensitive UV light photodetectors. The realization of such ultra-sensitive p-ZnS NR/ITO SBD detectors undoubtedly opens up new opportunities for diverse applications in nano-optics and nano-optoelectronics.

Acknowledgements

Electronic Supplementary Material: Supplementary material is available in the online version of this article at http://dx.doi.org/10.1007/s12274-014-0587-8.

References

[1] Monroy, E.; Omnès, F.; Calle, F. Wide-bandgap semiconductor ultraviolet photodetectors. *Semicond. Sci. Technol.* **2003**, *18*, R33–R51.

[2] Hadfield, R. H. Single-photon detectors for optical quantum information applications. *Nat. Photonics* **2009**, *3*, 696–705.

[3] Katz, J. Detectors for optical communications: A review. *TDA Progress Report* **1983**, *42–75*, 21–38.

[4] Bai, X.; Liu, H.-D.; McIntosh, D. C.; Campbell, J. C. High-detectivity and high-single-photon-detection-efficiency 4H-SiC avalanche photodiodes. *IEEE J. Quantum Elec.* **2009**, *45*, 300–303.

[5] Yan, F.; Xin, X. B.; Aslam, S.; Zhao, Y. G.; Franz, D.; Zhao, J. H.; Weiner, M. 4H-SiC UV photo detectors with large area and very high specific detectivity. *IEEE J. Quantum Elec.* **2004**, *40*, 1315–1320.

[6] Zhu, H.; Chen, X.; Cai, J.; Wu, Z. 4H-SiC ultraviolet avalanche photodetectors with low breakdown voltage and high gain. *Solid State Elec.* **2009**, *53*, 7–10.

[7] Verevkin, A.; Zhang, J.; Sobolewski, R.; Lipatov, A.; Okunev, O.; Chulkova, G.; Korneev, A.; Smirnov, K.; Gol'tsman, G. N.; Semenov, A. Detection efficiency of large-active-area NbN single-photon superconducting detectors in the ultraviolet to near-infrared range. *Appl. Phys. Lett.* **2002**, *80*, 4687–4689.

[8] Korneev, A.; Kouminov, P.; Matvienko, V.; Chulkova, G.; Smirnov, K.; Voronov, B.; Gol'tsman, G. N.; Currie, M.; Lo, W.; Wilsher, K.; et al. Sensitivity and gigahertz counting performance of NbN superconducting single-photon detectors. *Appl. Phys. Lett.* **2004**, *84*, 5338–5340.

[9] Xu, S.; Wang, Z. One-dimensional ZnO nanostructures: Solution growth and functional properties. *Nano Res.* **2011**, *4*, 1013–1098.

[10] Huang, K.; Zhang, Q.; Yang, F.; He, D. Ultraviolet photoconductance of a single hexagonal WO_3 nanowire. *Nano Res.* **2010**, *3*, 281–287.

[11] Luo, L. B.; Liang, F. X.; Jie, J. S. Sn-catalyzed synthesis of SnO_2 nanowires and their optoelectronic characteristics. *Nanotechnology* **2011**, *22*, 485701.

[12] Liu, Z.; Luo, T.; Liang, B.; Chen, G.; Yu, G.; Xie, X.; Chen, D.; Shen, G. High-detectivity InAs nanowire photodetectors with spectral response from ultraviolet to near-infrared. *Nano Res.* **2013**, *6*, 775–783.

[13] Kind, H.; Yan, H. Q.; Messer, B.; Law, M.; Yang, P. D. Nanowire ultraviolet photodetectors and optical switches. *Adv. Mater.* **2002**, *14*, 158–160.

[14] Jain, V.; Nowzari, A.; Wallentin, J.; Borgström, M. T.; Messing, M. E.; Asoli, D.; Graczyk, M.; Witzigmann, B.; Capasso, F.; Samuelson, L.; et al. Study of photocurrent generation in InP nanowire-based p–i–n photodetectors. *Nano Res.* **2014**, *7*, 1–9.

[15] Yang, C.; Barrelet, C. J.; Capasso, F.; Lieber, C. M. Single p-type/intrinsic/n-type silicon nanowires as nanoscale avalanche photodetectors. *Nano Lett.* **2006**, *6*, 2929–2934.

[16] Hayden, O.; Agarwal, R.; Lieber, C. M. Nanoscale avalanche photodiodes for highly sensitive and spatially resolved photon detection. *Nat. Mater.* **2006**, *5*, 352–356.

[17] Yan, R. X.; Gargas, D.; Yang, P. D. Nanowire photonics. *Nat. Photonics* **2009**, *3*, 569–576.

[18] Memis, O. G.; Katsnelson, A.; Kong, S.-C.; Mohseni, H.; Yan, M.; Zhang, S.; Hossain, T.; Jin, N.; Adesida, I. A photon detector with very high gain at low bias and at room temperature. *Appl. Phys. Lett.* **2007**, *91*, 171112.

[19] Memis, O. G.; Kohoutek, J.; Wu, W.; Gelfand, R. M.; Mohseni, H. Signal-to-noise performance of a short-wave infrared nanoinjection imager. *Opt. Lett.* **2010**, *35*, 2699–2701.

[20] Nie, B.; Hu, J. G.; Luo, L. B.; Xie, C.; Zeng, L. H.; Lv, P.; Li, F. Z.; Jie, J. S.; Feng, M.; Wu, C. Y.; et al.; Monolayer graphene film on ZnO nanorod array for high-performance Schottky junction ultraviolet photodetectors. *Small* **2013**, *9*, 2872–2879.

[21] González-Posada, F.; Songmuang, R.; Den Hertog, M.; Monroy, E. Room-temperature photodetection dynamics of single GaN nanowires. *Nano Lett.* **2012**, *2*,172–176.

[22] Yu, Y.; Jie, J.; Jiang, P.; Wang, L.; Wu, C.; Peng, Q.; Zhang, X.; Wang, Z.; Xie, C.; Wu, D.; et al. High-gain visible-blind UV photodetectors based on chlorine-doped n-type ZnS nanoribbons with tunable optoelectronic properties. *J. Mater. Chem.* **2011**, *21*, 12632–12638.

[23] Jiang, P.; Jie, J.; Yu, Y.; Wang, Z.; Xie, C.; Zhang, X.; Wu, C.; Wang, L.; Zhu, Z.; Luo, L. Aluminium-doped n-type ZnS nanowires as high-performance UV and humidity sensors *J. Mater. Chem.* **2012**, *22,* 6856–6561.

[24] Chen, R. S.; Chen, H. Y.; Lu, C. Y.; Chen, K. H.; Chen, C. P.; Chen, L. C.; Yang, Y. J. Ultrahigh photocurrent gain in m-axial GaN nanowires. *Appl. Phys. Lett.* **2007**, *91*, 223106.

[25] Calarco, R.; Marso, M.; Richter, T.; Aykanat, A. I.; Meijers, R.; Hart, A. V.; Stoica, T.; Lüth, H. Size-dependent photoconductivity in MBE-grown GaN-nanowires. *Nano Lett.* **2005**, *5*, 981–984.

[26] Jian, W.; Zhuang, J.; Zhang, D.; Dai, J.; Yang, W.; Bai, Y. Synthesis of highly luminescent and photostable ZnS:Ag nanocrystals under microwave irradiation. *Mater. Chem.*

[27] Yu, Y.; Zeng, L.; Jiang, Y.; Jie, J. Ultralow contact resistivity of Cu/Au with p-type ZnS nanoribbons for nanoelectronic applications. *IEEE Elec. Dev. Lett.* **2013**, *34*, 810–812.

[28] Soylu, M.; Yakuphanoglu, F. Photovoltaic and interface state density properties of the Au/n-GaAs Schottky barrier solar cell. *Thin Solid Films* **2011**, *519*, 1950–1954.

[29] Tuğluoğlu, N.; Yakuphanoglu, F.; Karadeniz, S. Determination of the interface state density of the In/p-Si Schottky diode by conductance and capacitance–frequency characteristics. *Phys. B* **2007**, *393*, 56–60.

[30] Okutan, M.; Basaran, E.; Yakuphanoglu, F. Electronic and interface state density distribution properties of Ag/p-Si Schottky diode. *Appl. Surf. Sci.* **2005**, *252*, 1966–1973.

[31] Kim, W.; Javey, A.; Vermesh, O.; Wang, O.; Li, Y. M.; Dai, H. J. Hysteresis caused by water molecules in carbon nanotube field-effect transistors. *Nano Lett.* **2003**, *3*, 193–198.

[32] Ghosh, T.; Basak, D. Nonvolatile memory effect in a Au/Cu-ZnO/p-Si type of metal–insulator–semiconductor structure. *IEEE Elec. Dev. Lett.* **2011**, *32*, 1746–1748.

[33] Sze, S. M.; Ng, K. K. *Physics of Semiconductor Devices*. Wiley-Interscience: New Jersey, 2007.

[34] Schroder, D. K. *Semiconductor Material and Device Characterization*. John Wiley & Sons, Inc.: New Jersey, 2006.

[35] Katz, O.; Garber, V.; Meyler, B.; Bahir, G.; Salzman, J. Gain mechanism in GaN Schottky ultraviolet detectors. *Appl. Phys. Lett.* **2001**, *79*, 1417–1419.

[36] Katz, O.; Bahir, G.; Salzman, J. Persistent photocurrent and surface trapping in GaN Schottky ultraviolet detectors. *Appl. Phys. Lett.* **2004**, *84*, 4092–4094.

Phys. **2006**, *99*, 494–497.